Investigating the nature of line broadening in electrochemically delithiated Li1.2Mn0.4Ni0.3Co0.1O2

Whitfield, Pamela; Niketic, Svetlana; Le Page, Yvon; Davidson, Isobel

Publisher's version / Version de l'éditeur:

International Centre for Diffraction Data (ICDD), 48, pp. 149-155, 2006

NRC Publications Record / Notice d'Archives des publications de CNRC:
https://nrc-publications.canada.ca/eng/view/object/?id=35de3390-e9e2-411e-883b-e615caf7d1e8
https://publications-cnrc.canada.ca/fra/voir/objet/?id=35de3390-e9e2-411e-883b-e615caf7d1e8

INVESTIGATING THE NATURE OF LINE BROADENING IN ELECTROCHEMICALLY DELITHIATED $Li_{1.2}Mn_{0.4}Ni_{0.3}Co_{0.1}O_2$

P.S. Whitfield, S. Niketic, Y. Le Page and I.J. Davidson

Institute for Chemical Process and Environmental Technology, National Research Council Canada, 1200 Montreal Road, Ottawa, Ontario, K1A 0R6, Canada

ABSTRACT

The anomalous line broadening behaviour exhibited by $Li_{1.2}Mn_{0.4}Ni_{0.3}Co_{0.1}O_2$ during charging to high voltage (> 4.4V) has been investigated. Previous hypotheses attributing the phenomena to stacking faults can not explain all of the broadening features, as some of them (e.g. 003) disobey the selection rules expected of stacking faults in a cubic close-packed system (H-K = 3N ± 1). An alternative explanation has been developed, that describes the broadening in terms of an inhomogeneity of the residual lithium within the crystal structure. The *hkl* dependence of the broadening has been formulated in a reciprocal space relationship dependant on the c reciprocal space vector, *L*, and the distribution of lithium in the material δ. It was found that the observed asymmetry can be modelled using the same *hkl* relationship. The *hkl*-dependant broadening and asymmetry corrections have been added to Topas script files for structural Rietveld refinements in the R-3m space group. The inhomogeneity approach produced profile fits very similar to those obtained using a model-independent spherical harmonics correction for both broadening and asymmetry. This would suggest that lithium inhomogeneity is the dominant cause of broadening in these samples.

INTRODUCTION

Lithium-ion batteries have largely replaced nickel-cadmium and nickel-metal hydride batteries for consumer electronics applications. Ever increasing energy demands are being made by smaller and smaller devices. The increased energy density of lithium-ion technology has made them a natural successor in this market. Lithium ion batteries rely on the 'shuttling' of lithium ions between a positive cathode material and negative anode on charge and discharge. The deintercalation and intercalation processes have to be highly reversible to obtain long service life. One of the more costly components of a lithium-ion battery is the cathode material, usually a lithiated transition metal oxide such as $LiCoO_2$. These materials have a layered structure for

easy extraction and insertion of lithium ions into the structure. Recently lithium-rich phases containing significant amounts of manganese have become the subject of much interest (1; 2). One such composition is $Li_{1.2}Mn_{0.4}Ni_{0.3}Co_{0.1}O_2$, which is a solid solution of Li_2MnO_3 and $LiNi_{0.75}Co_{0.25}O_2$. The materials exhibit unexpectedly high discharge capacities, and there is obvious interest in the structural stability of the materials during cycling. *In-situ* and *ex-situ* diffraction studies are a natural technique to use to study structural changes that occur during the removal and reinsertion of lithium into the material.

EXPERIMENTAL

$Li_{1.2}Mn_{0.4}Ni_{0.3}Co_{0.1}O_2$ was prepared using a sucrose-based chelation-combustion process (3) which has similarities to the Pechini method (4). The metal nitrates and/or acetates were dissolved in an aqueous solution where the pH had been reduced to approximately 1 using nitric acid. Water was removed by heating on a hotplate until a viscous brown liquid had been formed. At this stage the heating was increased to char and foam the mixture. Ultimately the carbonaceous matrix formed spontaneously combusts, producing a fine ash. This ash was heated in a furnace in air at 800ºC for 6 hours.

The powder was used to create electrodes by casting a mixture of active material, high surface area carbon and a polyvinylidene difluoride (PVDF) based binder. After drying, punched electrodes were assembled into 2325 coin cells versus lithium foil anodes using a polypropylene-based separator and an electrolyte solution of 1M $LiPF_6$ in ethylene carbonate/dimethyl carbonate. The cells were charged at constant rate between 2.0 and 4.6 volts until the required state-of-charge had been reached. The electrodes were extracted from the coin cells in a glove box, and the cathode material washed repeatedly with dimethyl carbonate before drying under vacuum. A chemical analysis of the material was not possible with the equipment available, due to the very small amount of material extracted from a single cell.

X-ray diffraction data were obtained using a twin-mirror parallel-beam Bruker D8. The specimens were mounted on silicon zero background holders and data collected between 5 and 100º 2θ. The data were analysed using a beta version of Topas 3.0 (5). A single X-ray diffraction dataset is insufficient to refine four cations, especially so as Mn, Ni and Co are very similar scatterers. Consequently the ratios of the transition metals Mn:Ni:Co were fixed to the nominal values of 0.500:0.375:0.125. The total site occupancies were constrained to equal one,

although the total transition metal to lithium ratio was freely refined. The effect of stacking faults on line profiles in reciprocal space were modelled using the program STACK (6).

RESULTS AND DISCUSSION

Portions of the raw data obtained during two full charge-discharge cycles are shown in Figure 1. Although significant changes are also apparent in other parts of the patterns the 003, 018, 110 and 113 (R-3m setting) reflections show most of the relevant features. It is clear that large changes occur in the lattice parameters during charge and discharge, as would be expected during oxidation and reduction of the transition metals within the lattice.

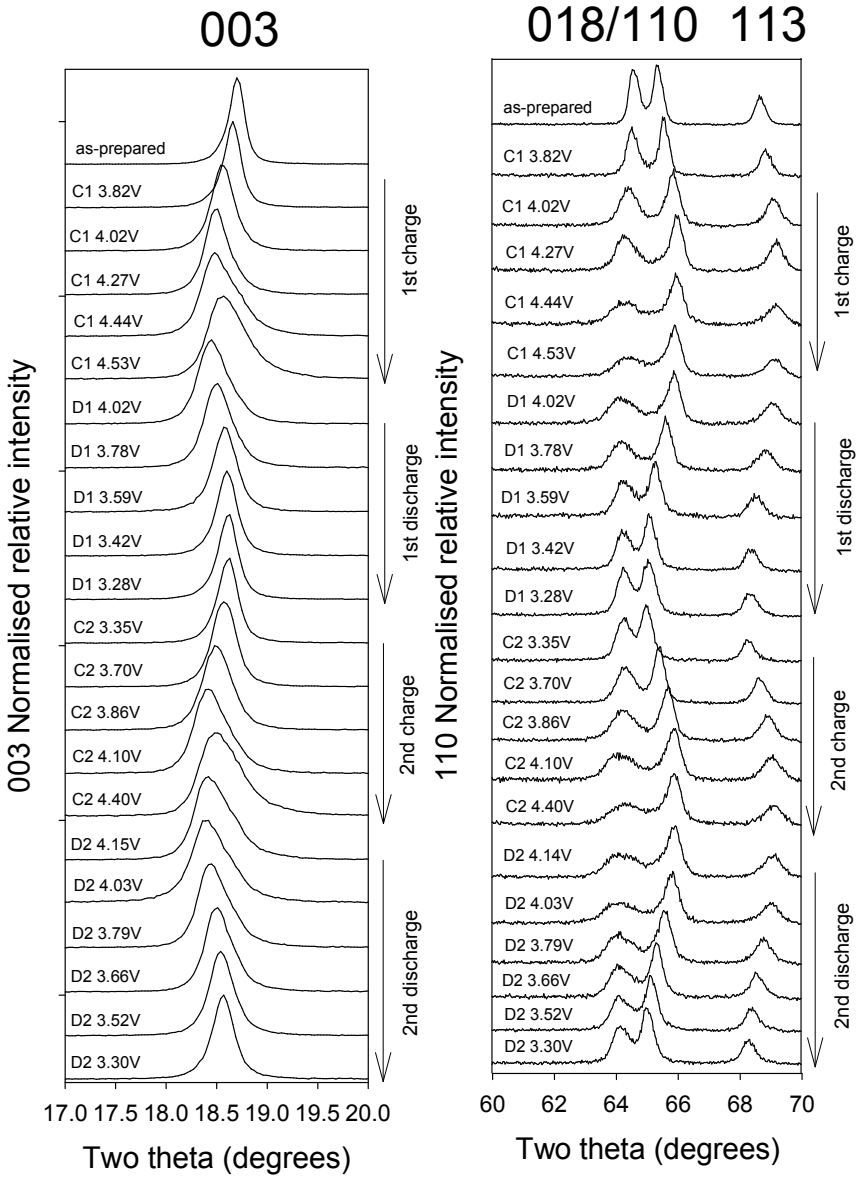

Figure 1. Behaviour of the R-3m 003, 018, 110 and 113 reflections during two full charge/discharge cycles

However, there are additional features including line broadening and asymmetry, which severely complicate analysis of the data. Without accurately modelling the peak profiles, any attempt at Rietveld analysis will not produce useful results. Figure 2 shows the fit to data at the end of first charge with serious misfits and unreasonably long metal-to-oxygen bond lengths for a highly oxidised material. A common technique for graphically examining *hkl* dependence of peak broadening is the Williamson-Hall plot (7). Such a plot for the diffraction data at the end of charge and discharge for the first two cycles is shown in Figure 3. It is apparent that the changes in broadening are highly reversible, and dependent solely on the *c* direction.

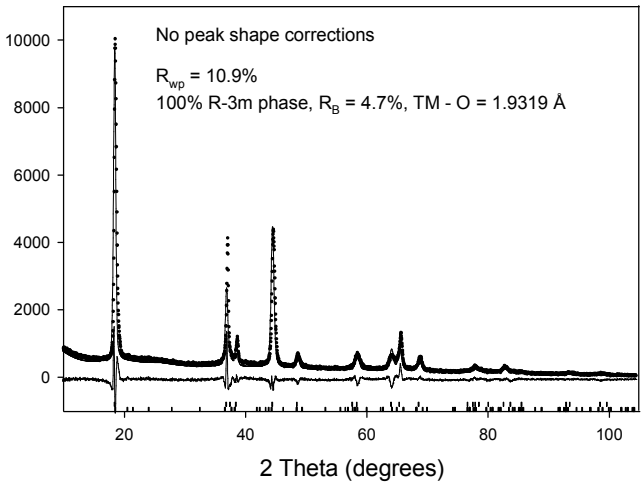

Figure 2. Rietveld difference plot of a fit to a R-3m structure model with no peak shape corrections

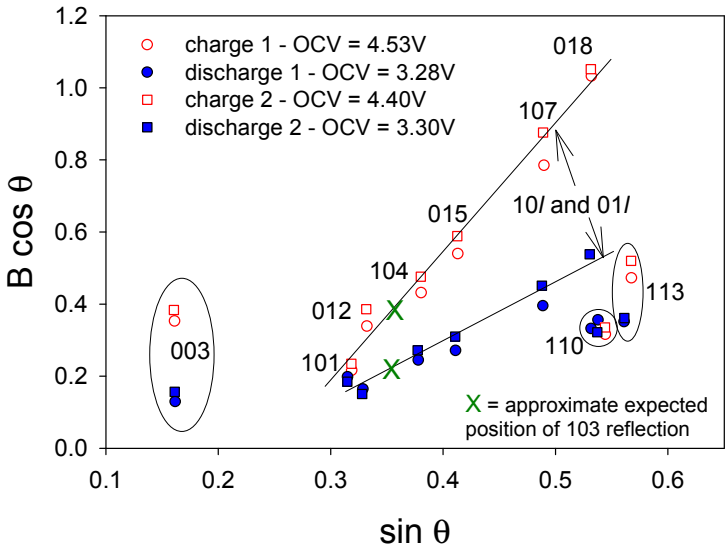

Figure 3. A Williamson-Hall plot showing the broadening of reflections at the end of charge and discharge for the first two full cycles. The Miller indices are those of the R-3m unit cell.

Although the as-prepared $Li_{1.2}Mn_{0.4}Ni_{0.3}Co_{0.1}O_2$ has a monoclinic C2/m symmetry, after the end of first charge, all of the reflections can be indexed on a closely-related simple R-3m cell. The R-3m structure has a cubic close-packed (ccp) oxygen lattice, and as such *hkl* selection rules exist to indicate what reflections will be affected by stacking faults (8). For a ccp lattice, where H-K = 3N ± 1, line broadening will occur, whilst other reflections will be unaffected. In the ccp system stacking faults may be classified as either deformation or twin faults, and according to the terminology of Warren (8); the probabilities of these faults are known as α and β respectively. Both types of fault follow the same selection rules as to whether broadening will happen or not, but the nature of the broadening differs in each case. Figure 4 shows the simulated broadening along c* for 5% of deformation and twin faults respectively, which shows that although the behaviour of the deformation faults is more complex, the same selection rules apply.

As is clearly shown in Figure 3, the 003 and 113 reflections broaden, whereas Figure 4 shows that this can not be due to stacking faults. Another possible source for broadening in such a layered structure could be inhomogeneity in the distribution of the residual lithium in the crystal structure. This can be described by the relationship:

$2q \times \delta \times Lc^* \times \cos(c^* \wedge R^*)$

where c* and R* are reciprocal space vectors, *L* is the reflection's miller index, q is a small constant, and δ refers to the lithium distribution where $x_0 - \delta < x_i < x_0 + \delta$.

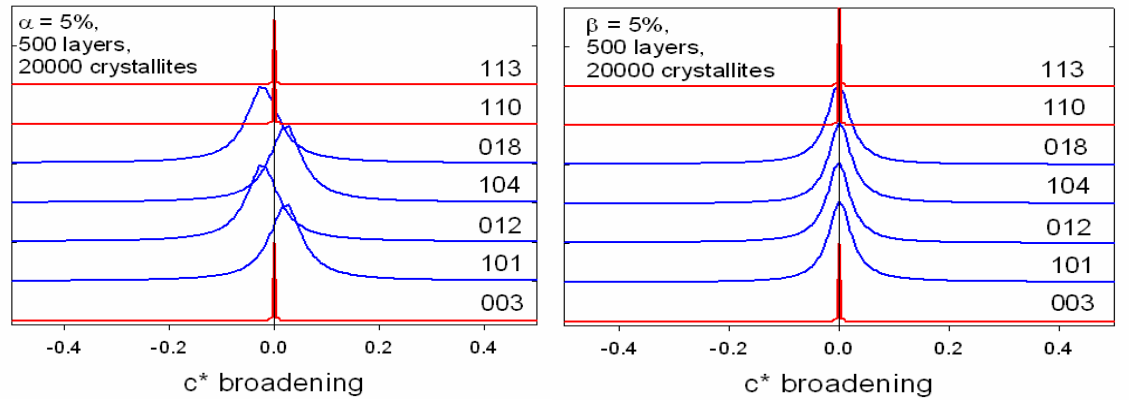

Figure 4. Simulated broadening along *c reciprocal space vector for (a) 5% deformation faults and (b) 5% twin faults**

However, this reciprocal space relationship does not explain the peak asymmetry observed. This may be due to either a real asymmetry in the lithium distribution of the material, or non-linearity in the *c* lattice parameter with lithium content. Figure 5 shows that the latter is true in this material, as the *c* parameter suddenly shrinks at the end of charge when the lithium content is very low.

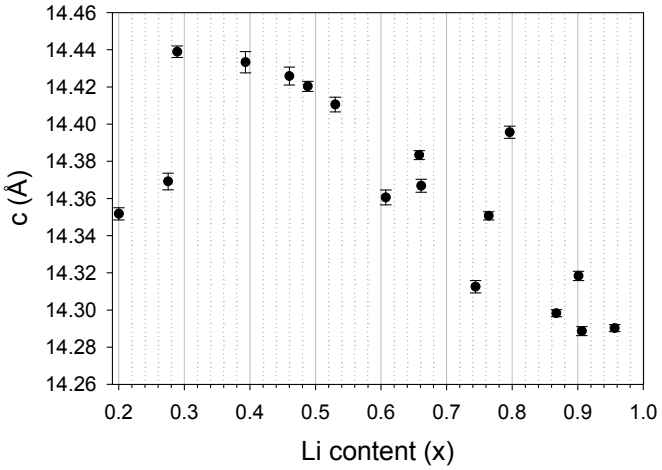

Figure 5. Dependence of *c* lattice parameter on the calculated residual Li in the active material. Scatter in the data is caused largely by errors in the quantitative analysis of the inactive portion of the $Li_{1.2}Mn_{0.4}Ni_{0.3}Co_{0.1}O_2$ in the electrode.

A combination of the two effects probably contributes to the overall peak shapes. The similarity of the fits shown in Figure 6(a) and (b) demonstrate the effectiveness of the peak-shape

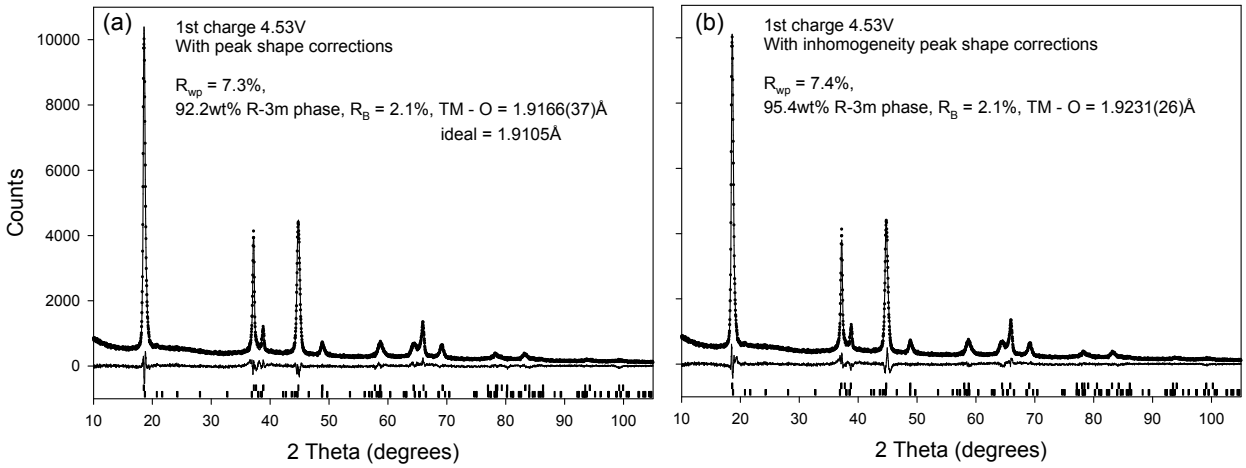

Figure 6. Rietveld difference plots with (a) spherical harmonics peak shape corrections and (b) reciprocal space lithium inhomogeneity peak shape corrections

corrections in a full structural Rietveld refinement. Both the spherical harmonics and inhomogeneity corrections allow for an accurate extraction of peak intensity compared to the uncorrected profiles (Figure 2). They both lead to similar fits to the data and yield similar bond distances that are within the range expected for a highly oxidised $Mn_{0.5}Ni_{0.375}Co_{0.125}O_2$. Unfortunately with a single dataset, the number of cations present precludes the refinement of detailed site compositions. The transitional metal ratio has to be assumed, and fixed for each of the sites. Only the transition metal to lithium ratio can realistically be refined. However, the

different metal-oxygen bond lengths (from bond valence) of Mn^{4+} (1.906Å) and Ni^{4+} (1.930Å) and Co^{4+} (1.870Å), do allow for a consistency check to be made, using the refined bond lengths and the site occupancies.

Rapid chemical deintercalation has been shown to produce the same broadening behaviour (9) described here. However, recent studies using very low charging rates showed significantly less broadening and asymmetry in the 003 reflection (10), suggesting that the inhomogeneity is not thermodynamically stable, and will vary according to the charge/discharge conditions used.

CONCLUSIONS

It has been demonstrated that conventional ccp stacking faults cannot be the primary cause of the line broadening and asymmetry observed in the *ex-situ* diffraction patterns of $Li_{1.2}Mn_{0.4}Ni_{0.3}Co_{0.1}O_2$ delithiated electrochemically to 4.6V at 10mA/g rate. It is suggested that a model based on inhomogeneity of the residual lithium in the crystal structure can model the observed profiles just as well as a model-independent spherical harmonics approach. Implementing the model in the Topas software allows structural information to be extracted using the Rietveld method that might otherwise be irretrievable.

REFERENCES

[1] Storey, C.; Kargina, I.; Grincourt, Y.; Davidson, I.J.; Yoo, Y.; Seung, D.Y., J.Power Sources, 2001, 97-98**,** 541-544.

[2] Lu, Z.; Dahn, J.R., J.Electrochem.Soc., 2002, 149**,** A815-822.

[3] Whitfield, P.S.; Niketic, S.; Davidson, I.J., J.Power Sources, 2005, 146**,** 617-621.

[4] Lessing, P.A., American Ceramic Society Bulletin, 1989, 68**,** 1002-1007.

[5] Bruker AXS (2005) *TOPAS V3: General profile and structure analysis software for powder diffraction data.* User Manual,

[6] STACK. Le Page,Y. (2005) available from yvon.le_page@nrc.gc.ca.

[7] Williamson, G.K.; Hall, W.H., Acta Metallurgica, 1953, 1**,** 22-31.

[8] Warren, B.E. (1969). *X-Ray Diffraction*, Reading, Mass, USA: Addison-Wesley Publishing Company Inc.

[9] Whitfield, P. S.; Niketic, S.; Davidson, I. J., Abstract 194, Battery and Energy Technology Joint Session, 207th Electrochemical Society Meeting, Quebec City, 15-20 May 2005

[10] Croguennec, L.; Weill, F.; Tran, N.; Martin, N.; Jordy, C.; Biensen, Ph.; Ménétrier, M.; Delmas, C., Abstract 49, International Meeting on Lithium Batteries, Biarritz, France, 18-23 June 2006